

PAPER • OPEN ACCESS

Asymmetry in the propagation of vortex domain wall artificial skyrmion composite system

To cite this article: D Eilmsteiner *et al* 2021 *J. Phys.: Condens. Matter* **33** 185803

View the [article online](#) for updates and enhancements.



IOP | ebooks™

Bringing together innovative digital publishing with leading authors from the global scientific community.

Start exploring the collection—download the first chapter of every title for free.

Asymmetry in the propagation of vortex domain wall artificial skyrmion composite system

D Eilmsteiner^{1,*}, Xi-guang Wang², L Chotorlishvili³, S Paischer¹, M Hoffmann¹, P Buczek⁴ and A Ernst^{1,5}

¹ Institute for Theoretical Physics, Johannes Kepler University Linz, 4040 Linz, Austria

² School of Physics and Electronics, Central South University, Changsha 410083, People's Republic of China

³ Institute für Physik, Martin-Luther Universität Halle-Wittenberg, D-06120 Halle/Saale, Germany

⁴ Department of Engineering and Computer Sciences, Hamburg University of Applied Sciences, Berliner Tor 7, 20099 Hamburg, Germany

⁵ Max Planck Institute of Microstructure Physics, 06120 Halle, Germany

E-mail: david.eilmsteiner@jku.at

Received 21 December 2020, revised 19 February 2021

Accepted for publication 12 March 2021

Published 23 April 2021



Abstract

We studied the propagation of an artificial skyrmion coupled to the vortex domain wall (VDW). We discovered the following effect: depending on the propagation's direction, the dynamics of the coupled skyrmion VDW can be faster than the isolated VDW's velocity. The reason for such behavior is the structural distortion that occurs in the coupled system. We interpret the numerical results in terms of the modified Thiele's equation. In particular, increasing the Thiele's equation counteractive coefficient leads to the perfect fitting with the micromagnetic simulation results.

Keywords: skyrmion, Landau–Lifshitz–Gilbert equation, micromagnetics

(Some figures may appear in colour only in the online journal)

1. Introduction


It is always fascinating when an appealing mathematical concept meets the real physical world. The skyrmion [1] is a topological soliton playing a crucial role in quantum field theory. Belavin and Polyakov [2] showed that the topological action of the field theory $S_{\text{top}}(\mathbf{n}) = \frac{i\theta}{4\pi} \int dx_1 dx_2 \mathbf{n} \cdot (\partial_1 \mathbf{n} \times \partial_2 \mathbf{n})$ and associated topological charge $W = \frac{1}{i\theta} S_{\text{top}}(\mathbf{n})$ are invariant with respect to the infinitesimal operations of the $O(3)$ group. Here θ is the topological angle, and $\mathbf{n}(x_1, x_2)$ is the vector field $\mathbf{r} = (x_1, x_2)$. Bogdanov was one of the first who uncovered the link between skyrmions and magnetism [3] and showed that a

magnetic texture $\mathbf{m}(\mathbf{r}) \equiv \mathbf{n}$ plays the role of the vector field. Nowadays, magnetism is a platform for testing fundamental physical concepts [4–22].

Formation of a magnetic skyrmion requires many criteria and conditions. Therefore natural skyrmions are rare and may exist only in a few materials for a limited set of parameters. Artificial skyrmions are objects obtained through a nanopatterning procedure. Typically for nanopatterning, one has to consider a bi-layer system. The upper layer possesses a nontrivial ground state magnetic texture and couples to the bottom layer through exchange interaction. The nontrivial magnetic surface in the top layer facilitates the formation of the skyrmion texture in the bottom layer. Thus skyrmions artificially can be formed in the absence of the Dzyaloshinskii–Moriya (DM) interaction [23].

The topological structure of skyrmions is useful for memory storage and logic devices. To move a skyrmion, one

* Author to whom any correspondence should be addressed.

 Original content from this work may be used under the terms of the [Creative Commons Attribution 4.0 licence](https://creativecommons.org/licenses/by/4.0/). Any further distribution of this work must maintain attribution to the author(s) and the title of the work, journal citation and DOI.

needs less effort than for a domain wall using standard tools such as the spin-polarized current, magnonic spin current, or inhomogeneous electric field gradient [24]. However, a skyrmion trajectory is not parallel to the applied torque but has an orthogonal component. The reason for the drift in the orthogonal direction is the skyrmion Hall effect. Skyrmion and antiskyrmion possess opposite topological charges. The total charge of the bi-skyrmion constructed from the coupled skyrmion–antiskyrmion pair is zero. Therefore bi-skyrmions do not experience a Magnus force and their trajectory is a straight-line [25].

Recently, the following setup has been proposed for the generation of artificial skyrmions [23]: A circular nano-dot is placed on the top of coupled thin layers. The geometry influences the magnetization profile in the nano-dot. In particular, the circular geometry generates a stable vortex state in the nano-dot and creates a bi-skyrmion state in the bottom coupled thin layers. This artificial bi-skyrmion structure exploits a sophisticated nanofabrication technique for the generation of the circular nano-dot. Nevertheless, the proposed setup is not suited to drag the bi-skyrmion. The bi-skyrmion is firmly pinned in the region of the circular nano-dot.

Thus, already existing schemes for creating artificial skyrmions exploit the conditions breaking down the mobility of skyrmions, while the objective is to have artificial skyrmions with high mobility features. We propose an experimentally feasible model of an artificial skyrmion coupled with a vortex domain wall (VDW). We will show that the artificial skyrmion connected to the VDW possesses high mobility features and a certain asymmetry in the propagation in opposite directions.

The work is organized as follows: in section 2, we describe the model, in section 3 we discuss mechanisms of the formation of bi-skyrmion structures, in section 4 we study the coupled motion of the artificial skyrmion and VDW. We demonstrate our main finding: directional helical asymmetry of the velocity of coupled system and conclude the work. In section 5 we summarise the work.

2. Model

In the present work, we consider two types of systems with different geometries. In the first model the Co nanodisks of the circular shape and vortex magnetization profile are attached to the SrRuO₃–La_{0.7}Sr_{0.3}MnO₃ bi-layer system (termed SRO–LSMO in what follows). The skyrmion–antiskyrmion pair is formed in the SRO–LSMO bilayer. This structure is shown in figure (1). In this model, the artificial skyrmion is pinned with the nanodisk, and the skyrmion is immobile. To study the motion of skyrmions, we propose the second model. In particular, we propose the model of an artificial skyrmion in the Co–CoPt bilayer interface system without DM interaction. The VDW from the track layer stabilizes an artificial skyrmion in the CoPt layer. The magnetocrystalline anisotropy in the layers is out of the plane. Layers are coupled with each other by the exchange interaction. An applied spin-polarized torque drives the VDW, and the skyrmion follows the VDW. Thus, the artificial skyrmion is coupled to the vortex wall and moves together with it. The second model is analyzed in section 4.

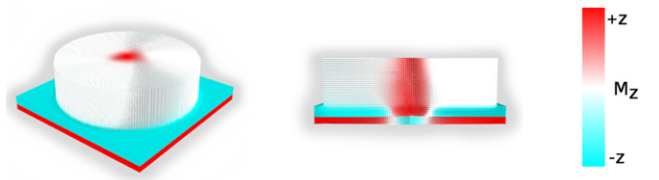


Figure 1. The setup (left) and sectional view (center) through the disk and the layers. The color code defines the z component of the local magnetization. The Co vortex disk placed on the SRO–LSMO bilayer creates the skyrmion–antiskyrmion pair in the SRO–LSMO bilayer system.

The second model does not require nanofabrication of nano-dots, and this is a clear advantage. Besides, the mechanism for moving the VDW and the artificial skyrmion is experimentally feasible. Furthermore, the magnetic skyrmion Hall effect is entirely suppressed in our scheme, which is significant for applications based on a fully controlled skyrmion motion.

In the micromagnetic simulations, the magnetic dynamics of the n th layer $\mathbf{M}_n(\mathbf{r}) = M_s \mathbf{m}_n(\mathbf{r})$, (where M_s is the saturation magnetization) is governed by the Landau–Lifshitz–Gilbert equation

$$\frac{\partial \mathbf{M}_n}{\partial t} = -\gamma \mathbf{M}_n \times \left(\mathbf{H}_n^{\text{eff}} - \frac{1}{\mu_0 M_s} \frac{\delta E}{\delta \mathbf{m}_n} \right) + \frac{\alpha}{M_s} \mathbf{M}_n \times \frac{\partial \mathbf{M}_n}{\partial t}. \quad (1)$$

Here γ is the gyromagnetic ratio and α is the phenomenological Gilbert damping constant, E is the inter-layer exchange energy with coupling parameters J_{12} and J_{23} .

The effective field $\mathbf{H}_n^{\text{eff}}$ consists of the intra-layer exchange field, the demagnetization field $\mathbf{H}_{\text{demag}}$, the anisotropy field, and of the applied external magnetic field, $\mathbf{H}_n^{\text{eff}} = \frac{2A_n^{\text{ex}}}{\mu_0 M_s} \nabla^2 \mathbf{m}_n + H_z \mathbf{z} + 2K_n^\beta m_n^\beta + \mathbf{H}_{\text{demag}}$, where A_n^{ex} is the exchange stiffness, K_n^β , $\beta = x, y, z$ is the magnetic anisotropy, H_z is the external magnetic field applied along the z -direction. The demagnetization field is given by [26]

$$\mathbf{H}_{\text{demag}}(\mathbf{r}) = -\frac{M_s}{4\pi} \int_V \nabla \nabla' \cdot \frac{1}{\mathbf{r} - \mathbf{r}'} \mathbf{m}(\mathbf{r}') d\mathbf{r}'. \quad (2)$$

For micromagnetic simulations we exploit the object-oriented micromagnetic framework (OOMMF) [27]. The formation of a skyrmion is verified through the topological charge figures (2) and (3). We note that there are two different types of domain walls in the magnetic nanowires: the transverse wall (TW) and the VDW, see [28–31]. Depending on the geometry of the sample, TW and VDW exhibit different diverse stability and robustness. TWs have a relatively simple structure. Schryer N L and Walker [32] proposed an analytical description of the TW. This approach allows estimation of the critical threshold velocity and the strength of the spin-polarized current, above which the TW is not stable. Walker’s trial function has the form [32]

$$\phi(x) = \tan^{-1} \exp\left(\frac{x}{\Delta}\right), \quad \theta(x) = \frac{\pi}{2}. \quad (3)$$

Here $\phi(x)$, $\theta(x)$ are the angles between the direction of the magnetization and the nanowire (aligned along the $+X$ axis),

Δ is the width of the domain wall. Taking into account Walker’s trial function equation (3) for the velocity of the TW one obtains [28]

$$v_x = \frac{\gamma H \Delta}{\alpha} - \frac{c_J}{\alpha}, \quad (4)$$

where H is the external magnetic field, and c_J is the amplitude of the spin-polarized electron current. The motion of the VDW is sophisticated, and the equation for the velocity components read:

$$\begin{aligned} -G_v v_y + D_v(\alpha v_x + c_J) &= 0, \\ G_v(v_x + b_J) + \alpha D_v v_y &= 0. \end{aligned} \quad (5)$$

Here G_v is the domain gyro-coupling vector, D_v is the domain dissipation dyadic tensor, $b_J = c_J/\xi$ with nonadiabaticity coefficient ξ (see [28] for more details). According to Walker’s breakdown, when VDW’s velocity exceeds the critical threshold value, VDW converts into the more trivial TW. The mechanism of this transformation is described in [28]. We note that the result equation (5) from [28] does not include two factors: (i) the coupling force between top VDW and bottom skyrmion (ii) the out-of-plane spin-transfer torque. Including these two factors, we generalize equation (5) in section 4.

3. Generation of artificial bi-skyrmions

The main challenge in skyrmionics is reaching both topological and thermal stability. The probability of collapsing of skyrmions follows the Arrhenius law. When the potential barrier is higher than the thermal energy, the skyrmion is stable. However, at high temperatures, thermal fluctuations may cause a thermal collapse of the skyrmion [33]. Among the materials hosting natural skyrmions due to the strong DM interaction, a paradigmatic example is the chiral magnet MnSi. An interplay between anisotropy, external fields, ferromagnetic exchange interaction, and most crucially, the DM interaction determines stability and the size of skyrmion configurations [34]. Natural materials rarely fulfill these conditions. However, exploiting inter-material coupling grants stable artificial skyrmion textures in natural materials without DM interaction.

We prove that a vortex disk [35] positioned on a bi-layer generates and stabilizes an artificial bi-skyrmion magnetic texture, i.e., a skyrmion–antiskyrmion pair (see figure 1). Bi-skyrmions are of great interest as they, possessing vanishing total topological charge, do not experience the skyrmion Hall effect [36]. A disk made of Co (radius 45 nm, height 24 nm, exchange stiffness $A = 1.9 \times 10^{-11} \text{ J m}^{-1}$, saturation magnetization $M_s = 1.4 \times 10^6 \text{ A m}^{-1}$) [37] in which shape anisotropy stabilizes the vortex is placed on the SRO–LSMO bi-layer (heights 6 nm and 4 nm; exchange stiffnesses $A = 1.8 \times 10^{-12} \text{ J m}^{-1}$ and $A = 5.46 \times 10^{-12} \text{ J m}^{-1}$; saturation magnetizations $M_s = 0.2 \times 10^6 \text{ A m}^{-1}$ and $M_s = 0.56 \times 10^6 \text{ A m}^{-1}$; anisotropy constants $K = 6.4 \times 10^5 \text{ J m}^{-3}$ and $K = -2 \times 10^3 \text{ J m}^{-3}$ respectively) [38]. The inter-layer coupling strengths are treated as free parameters throughout the micromagnetic simulations performed

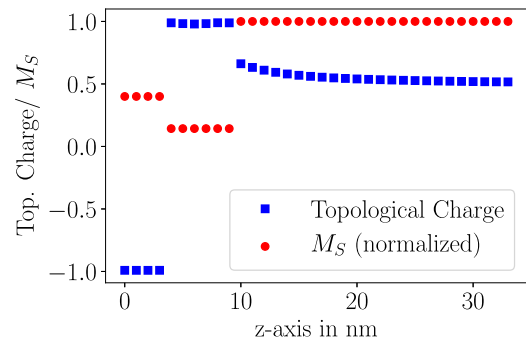


Figure 2. Topological charge in the planes perpendicular to the z -direction once the bi-skyrmion is created: in the LSMO (SRO) layer an antiskyrmion (skyrmion) with topological charge -1 ($+1$) arises. Additionally the layers’ and disk’s saturation magnetization M_s (divided by the disk’s M_s) are depicted. Values of the inter-layer couplings $J_{12} = 5 \times 10^{-12} \text{ J m}^{-1}$, $J_{23} = -5 \times 10^{-12} \text{ J m}^{-1}$.

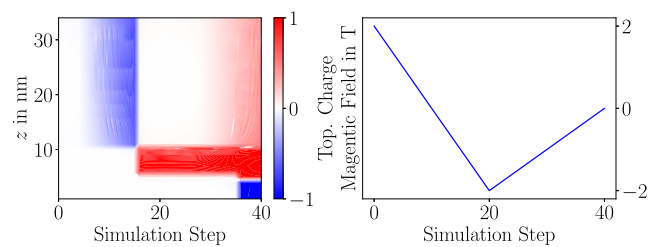


Figure 3. Topological charge in the system’s different areas throughout the bi-skyrmion’s creation process. The right-hand side graph depicts the corresponding applied field.

using OOMMF [27]. Their signs are fixed, imposing ferromagnetic coupling between the vortex disk and the first layer and antiferromagnetic coupling between the two layers. In particular, absolute values of the inter-layer couplings used in calculations $J_{12} = 5 \times 10^{-12} \text{ J m}^{-1}$, $J_{23} = -5 \times 10^{-12} \text{ J m}^{-1}$ are comparable with the intra-material exchange coupling.

Our scheme for the generation of textures of magnetic bi-skyrmions requires an external magnetic field (see figure 3). The magnetic field is applied perpendicular to the layers and varied step-wise from positive to negative values of $|B| \approx 2 \text{ T}$ and back to zero. The topological charge diagram figure (3) (the left figure) depicts the evolution of the charge during the variation with the corresponding applied fields (the right figure). We apply the conjugate gradient energy minimization procedure implemented in OOMMF at each step. When the non-trivial (nearly antiskyrmion) state in the vortex disk collapses, it produces a skyrmion in the adjacent layer. The antiskyrmion in the bottom layer is formed later, after the magnetic field approaches zero figure (2).

The vortex disk is a useful tool in numerics to highlight conditions and mechanisms of the formation and stability of artificial magnetic bi-skyrmion magnetic texture. However, for studying dynamic properties, i.e., skyrmion drag effect, we replace the vortex disk by the VDW.

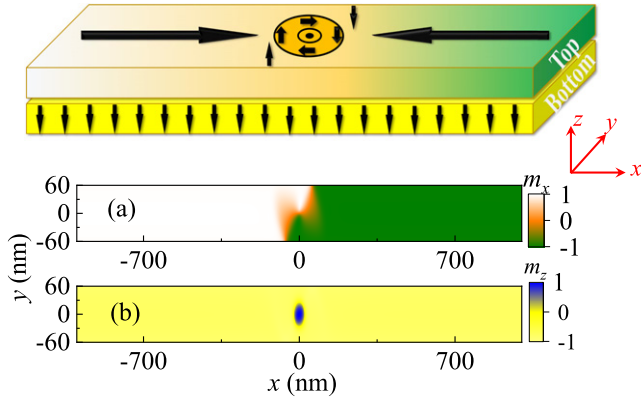


Figure 4. Top panel is the schematic of coupled VDW (chirality parameter $c = 1$) and artificial skyrmion. (a) and (b) are profiles of m_x (x component of local unit magnetization) in top layer and m_z (z component of local unit magnetization) in the bottom layer, respectively. The material parameters for top Co track: (exchange constant $A^{\text{Co}} = 2.5 \times 10^{-11} \text{ J m}^{-1}$, saturation magnetization $M_s^{\text{Co}} = 1.4 \times 10^6 \text{ A m}^{-1}$, and $\alpha = 0.04$) and bottom CoPt film (exchange constant $A^{\text{CoPt}} = 1.5 \times 10^{-11} \text{ J m}^{-1}$, saturation magnetization $M_s^{\text{CoPt}} = 5 \times 10^5 \text{ A m}^{-1}$, uniaxial anisotropy perpendicular to the film with constant $K_z^{\text{CoPt}} = 4 \times 10^5 \text{ J m}^{-3}$, and $\alpha = 0.04$) are used.

4. Coupled motion of VDW artificial skyrmion

Artificial skyrmions confined near the center of the nanodisk have low mobility. In the present work, we propose an alternative scheme. We place a nanostrip with a stable VDW on the top of the magnetic layer with out of plane anisotropy. The coupling to the VDW stabilizes an artificial skyrmion structure in the bottom magnetic layer, as demonstrated by figure 4. To move the VDW we exploit the electric current induced spin-transfer torque $b_J \mathbf{T}_s = b_J \mathbf{m} \times \mathbf{x} \times \mathbf{m}$ flowing in the neighboring heavy metal layer attached to the nanostripe. The VDW sets the artificial skyrmion in motion. We describe the underlying physical process through Thiele equations for the coupled motion of VDW ($q_{x,1}, q_{y,1}$) and skyrmion ($q_{x,2}, q_{y,2}$).

$$\begin{aligned} -G_v \partial_t q_{y,1} + \alpha D_{xx} \partial_t q_{x,1} + B_x &= F_x \\ -\kappa q_{y,1} + G_v \partial_t q_{x,1} + \alpha D_{yy} \partial_t q_{y,1} &= F_y, \\ +\alpha D_s \partial_t q_{x,2} - G_s \partial_t q_{y,2} &= -F_x, \\ +\alpha D_s \partial_t q_{y,2} + G_s \partial_t q_{x,2} &= -F_y. \end{aligned} \quad (6)$$

Parameters $G_v = -2\pi p$, $D_{yy} = D_v = -\pi \ln \frac{R}{a}$, $D_{xx} = D_v + D_t$, $D_t = -2\pi$ and $B_x = b_J c L$ characterize the vortex structure [28]. The spin orbit torque coefficient is given by $b_J = \frac{J_{\text{Co}} \gamma \hbar \theta_{\text{SH}}}{2\mu_0 e M_s t}$, where θ_{SH} is the spin-Hall angle, e is the electron charge, and t is the thickness of top layer. For the artificial skyrmion structure: $G_s = 4\pi p$ and $D_s = 4\pi$. The polarity of vortex wall and skyrmion are $p = 1$ throughout our study, while $c = \pm 1$ is the chirality of the vortex wall, R is the radius of the vortex core, and a is the lattice constant of the crystal structure. The scaling length is defined from $L = \int dV \mathbf{m} \times (\partial_x \mathbf{m} \times \mathbf{T}_s)$. The constant $\kappa = A^{\text{Co}} / (2\pi R^3)$ describes the counteractive force from the lateral boundary and depends on the details of the

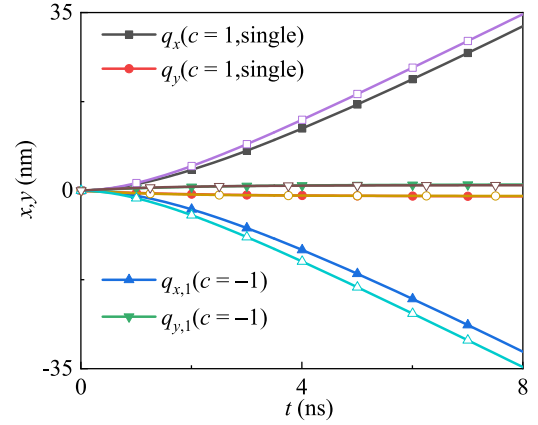


Figure 5. The motion of the VDW. The solid dots describe simulation results, and the open dots correspond to the Thiele's equation equation (6).

wall structure [28]. The coupling force between the top vortex wall and the bottom skyrmion [39, 40] is introduced by $F_{x(y)} = \eta \frac{q_{x(y),1} - q_{x(y),2}}{r}$, $\eta = \eta_0 \partial_r \exp(-\frac{r}{R})$ and $r = \sqrt{(q_{x,1} - q_{x,2})^2 + (q_{y,1} - q_{y,2})^2}$, and negative η_0 describes the coupling strength.

At first, we analyze the motion of the 'bare' VDW decoupled from the skyrmion. The velocity, in this case, is equal to $v_x = \frac{cb_J L_x}{\alpha[2\pi + \pi \ln(R/a)]}$ and y component of velocity is zero $\partial_t q_{y,1} = 0$. From micromagnetic simulation data, we obtain $L \approx 40 \text{ nm}$. For $\theta_{\text{SH}} = 0.1$, $J_{\text{Co}} = 2.7 \times 10^7 \text{ A cm}^{-2}$, and the value of the speed is $v_x = 5.3 \text{ m s}^{-1}$. The result obtained through Thiele's equation equation (6) is plotted in figure 5 and is in a good agreement with the result of micromagnetic simulations. The sign change of c inverts the motion direction while the speed is the same.

As a next step, we analyze the motion of the skyrmion coupled with the VDW. The coupling between the vortex and the skyrmion slightly distorts the vortex structure, leading to the larger scaling parameter $L \approx 90 \text{ nm}$ in equation (6). To explore the dynamics of the coupled system, we set the parameter $c = \pm 1$ and compare the result with the bare vortex wall. The Thiele's equation equation (6) shows that the coupled system moves in the same direction, with slightly lower velocity (figure 6(a)). Surprisingly micromagnetic calculations show left-right asymmetry when the sign of chirality of the VDW is inverted (figure 6(b)). For $c = -1$, the coupled system moves slower ($v_x = -3.6 \text{ m s}^{-1}$) as compared to the bare VDW. However, for $c = 1$, the dynamics of the coupled system become slightly faster ($v_x = 5.4 \text{ m s}^{-1}$) than the motion of the single VDW. Thus the chirality of the VDW coupled to the skyrmion system leads to an interesting phenomenon.

The asymmetry occurs due to reshuffling (distortion) of the VDW's internal structure. Considering the Thiele's equation parameters as phenomenological quantities, we tried to fit results governed by the Thiele's equation with the micromagnetic calculations. For example, the distortion affects the counteractive force from the lateral boundary and changes the value of κ when the vortex wall moves in the $+x$ direction (lateral drift is in $-y$ direction). When increasing κ by a factor 3, the motion of the coupled VDW and skyrmion becomes faster,

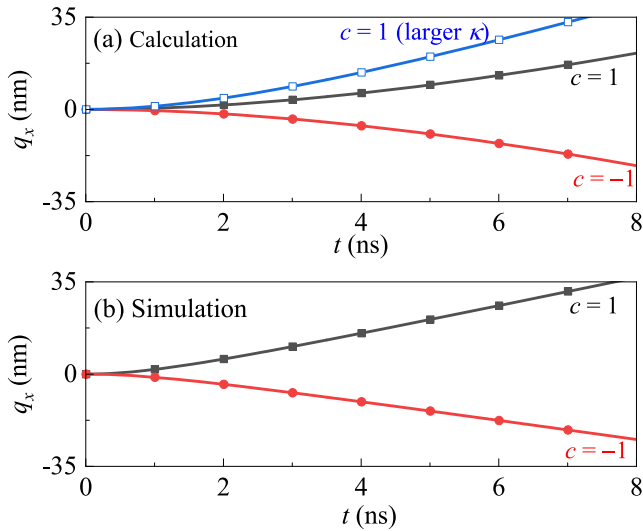


Figure 6. The motion of the coupled VDW and skyrmion. The skyrmion follows closely to the vortex wall, and $q_{x,1} = q_{x,2} = q_x$

see figure 6(a). For fitting the simulation results, we use the larger counteractive coefficient $\kappa_1 = 1.5\kappa$, and obtain $v_x = 5.4 \text{ m s}^{-1}$ when $c = 1$ from equation (6). When $c = -1$, the counteractive coefficient $\kappa_2 = 0.8\kappa$ is adopted for fitting $v_x = -3.6 \text{ m s}^{-1}$.

5. Conclusions

Formation of skyrmions requires specific conditions, and therefore natural skyrmions exist only in few materials. Thus the challenge for modern skyrmionics is the creation of artificial skyrmions and, on the other hand, ensuring a high mobility the artificial skyrmions. In the present work, we considered two types of systems with different geometries. In the first model, the Co nanodisks of the circular shape and vortex magnetization profile are attached to the SRO–LSMO bilayer, inducing a skyrmion–antiskyrmion pair in the bilayer. In the first model, the artificial skyrmion is pinned with the nanodisk, and the skyrmion is immobile. In the second model, the upper Co track is attached to the bottom layer with an artificial skyrmion, and the skyrmion is stabilized by the VDW placed in the upper Co track. The artificial skyrmion is coupled to the vortex wall and moves together with it. The second scheme ensures high mobility of the artificial skyrmion, and, what is essential, the skyrmion Hall effect is suppressed due to the counteractive force (k term) from the lateral boundary. This effect is similar to the case of a single vortex wall [28]. The trajectory of the artificial skyrmion is rectilinear, and this fact is beneficial for skyrmionic spintronics. We also showed that there is a left–right asymmetry in the VDW velocity when the sign of chirality of the VDW is inverted. This asymmetry occurs due to distortion of the internal structure of the VDW. The coupling with the bottom layer causes distortion, and chirality plays an important role. For $c = 1$ and $c = -1$, the distortions are different. By fitting the Thiele’s equation counteractive coefficient, we obtain a similar asymmetry. The slight change in the counteractive coefficient mimics the structural distortions in the VDW.

Acknowledgments

We thank G Tatara for useful discussions. This work was supported by the Shota Rustaveli National Science Foundation of Georgia (SRNSFG) (Grant No. FR-19-4049), the project W26000 Nanostrukturierte Materialien and the National Natural Science Foundation of China (Grant No. 11704415).

Data availability statement

All data that support the findings of this study are included within the article (and any supplementary files).

ORCID iDs

L Chotorlishvili <https://orcid.org/0000-0001-7042-9273>

M Hoffmann <https://orcid.org/0000-0002-8426-725X>

References

- [1] Skyrme T H R 1961 *Proc. R. Soc. A* **260** 127
- [2] Belavin A A and Polyakov A M 1975 *JETP Lett.* **22** 245
- [3] Wilson M N, Butenko A B, Bogdanov A N and Moncheshky T L 2014 *Phys. Rev. B* **89** 094411
- [4] Mhlbauer S, Binz B, Jonietz F, Pfleiderer C, Rosch A, Neubauer A, Georgii R and Böni P 2009 *Science* **323** 915
- [5] Dai Y Y, Wang H, Tao P, Yang T, Ren W J and Zhang Z D 2013 *Phys. Rev. B* **88** 054403
- [6] Kravchuk V P *et al* 2016 *Phys. Rev. B* **94** 144402
- [7] Seki S, Yu X Z, Ishiwata S and Tokura Y 2012 *Science* **336** 198
- [8] Iwasaki J, Beekman A J and Nagaosa N 2014 *Phys. Rev. B* **89** 064412
- [9] Ezawa Z F and Hasebe K 2002 *Phys. Rev. B* **65** 075311
- [10] Lian Y, Rosch A and Goerbig M O 2016 *Phys. Rev. Lett.* **117** 056806
- [11] Müller J, Rajeswari J, Huang P, Murooka Y, Ronnow H M, Carbone F and Rosch A 2017 *Phys. Rev. Lett.* **119** 137201
- [12] Liu Y-H, Li Y-Q and Han J H 2013 *Phys. Rev. B* **87** 100402(R)
- [13] Schütte C and Garst M 2014 *Phys. Rev. B* **90** 094423
- [14] White J S *et al* 2014 *Phys. Rev. Lett.* **113** 107203
- [15] Lin S-Z, Bulaeviskii L N 2013 *Phys. Rev. B* **88** 060404(R)
- [16] Wang C, Gong M, Han Y, Guo G and He L 2017 *Phys. Rev. B* **96** 115119
- [17] Kong L and Zang J 2013 *Phys. Rev. Lett.* **111** 067203
- [18] Derras-Chouk A, Chudnovsky E M and Garanin D A 2018 *Phys. Rev. B* **98** 024423
- [19] Haldar S, von Malottki S, Meyer S, Bessarab P F and Heinze S 2018 *Phys. Rev. B* **98** 060413(R)
- [20] Psaroudaki C and Loss D 2018 *Phys. Rev. Lett.* **120** 237203
- [21] Psaroudaki C, Hoffman S, Klinovaja J and Loss D 2017 *Phys. Rev. X* **7** 041045
- [22] Langner M C *et al* 2014 *Phys. Rev. Lett.* **112** 167202
- [23] Lin S-Z, Batista C D, Reichhardt C and Saxena A 2014 *Phys. Rev. Lett.* **112** 187203
- [24] Sun F, Ye J and Liu W-M 2017 *New J. Phys.* **19** 083015
- [25] van Hoogdalem K A, Tserkovnyak Y and Loss D 2013 *Phys. Rev. B* **87** 024402
- [26] Komineas S and Papanicolaou N 2015 *Phys. Rev. B* **92** 064412
- [27] Lin S-Z, Reichhardt C, Batista C D and Saxena A 2013 *Phys. Rev. B* **87** 214419
- [28] Müller J and Rosch A 2015 *Phys. Rev. B* **91** 054410
- [29] Koshibae W and Nagaosa N 2017 *Sci. Rep.* **7** 42645
- [30] Hrabec A *et al* 2017 *Nat. Commun.* **8** 15765

- [20] Cacilhas R, Carvalho-Santos V L, Vojkovic S, Carvalho E B, Pereira A R, Altbir D and Núñez Á S 2018 *Appl. Phys. Lett.* **113** 212406
- [21] Ang C C I, Gan W and Lew W S 2019 *New J. Phys.* **21** 043006
- [22] Zhou Y and Ezawa M 2014 *Nat. Commun.* **5** 4652
- [23] Miao B F *et al* 2015 *Appl. Phys. Lett.* **107** 222402
- [23] Sun L *et al* 2013 *Phys. Rev. Lett.* **110** 167201
- [24] Wang X-g, Chotorlishvili L, Guo G-h, Jia C-L and Berakdar J 2019 *Phys. Rev. B* **99** 064426
- [25] Takagi R, Yu X Z, White J S, Shibata K, Kaneko Y, Tatara G, Ronnow H M, Tokura Y and Seki S 2018 *Phys. Rev. Lett.* **120** 037203
- Yu X Z, Tokunaga Y, Kaneko Y, Zhang W Z, Kimoto K, Matsui Y, Taguchi Y and Tokura Y 2014 *Nat. Commun.* **5** 3198
- Wang W *et al* 2016 *Adv. Mater.* **28** 6887
- [26] Wang X-g, Chotorlishvili L, Guo G-h and Berakdar J 2018 *J. Appl. Phys.* **124** 073903
- [27] Donahue M J and Porter D G 1999 *Interagency Report NISTIR 6376*
- [28] He J, Li Z and Zhang S 2006 *Phys. Rev. B* **73** 184408
- [29] Leliaert J, Van de Wiele B, Vansteenkiste A, Laurson L, Durin G, Dupre L and van Waeyenberge B 2014 *Phys. Rev. B* **89** 064419
- [30] Min H, McMichael R D, Donahue M J, Miltat J and Stiles M D 2010 *Phys. Rev. Lett.* **104** 217201
- [31] Wieser R, Nowak U and Usadel K D 2004 *Phys. Rev. B* **69** 064401
- [32] Schryer N L and Walker L R 1974 *J. Appl. Phys.* **45** 5406
- [33] Wang X-G *et al* 2020 *npj Comput. Mater.* **6** 140
- [34] Buhrandt S and Fritz L 2013 *Phys. Rev. B* **88** 195137
- [35] Sun L *et al* 2013 *Phys. Rev. Lett.* **110** 167201
- [36] Zhang X, Zhou Y and Ezawa M 2016 *Nat. Commun.* **7** 10293
- [37] Miao B F *et al* 2015 *Appl. Phys. Lett.* **107** 22
- [38] Schaeffer A F, Chotorlishvili L, Maznichenko I V, Ernst A, Doerr K, Mertig I and Berakdar J 2018 *APL Mater.* **6** 076103
- [39] Tiwari K L, Lavoie J, Pereg-Barnea T and Coish W A 2019 *Phys. Rev. B* **100** 125414
- [40] Wang X-G *et al* 2020 *Phys. Rev. Lett.* **125** 227201